Kinematic dynamo action in a sphere. I
Effects of differential rotation and
meridional circulation on solutions
with axial dipole symmetry

By David Gubbins, C. N. Barber, S. Gibbons† and J. J. Love

Department of Earth Sciences, University of Leeds, Leeds LS2 9JT, UK

A sphere containing electrically conducting fluid can generate a magnetic field by dynamo action, provided the flow is sufficiently complicated and vigorous. The dynamo mechanism is thought to sustain magnetic fields in planets and stars. The kinematic dynamo problem tests steady flows for magnetic instability, but rather few dynamos have been found so far because of severe numerical difficulties. Dynamo action might, therefore, be quite unusual, at least for large-scale steady flows. We address this question by testing a two-parameter class of flows for dynamo generation of magnetic fields containing an axial dipole. The class of flows includes two completely different types of known dynamos, one dominated by differential rotation (D) and one with none. We find that 36% of the flows in seven distinct zones in parameter space act as dynamos, while the remaining 64% either fail to generate this type of magnetic field or generate fields that are too small in scale to be resolved by our numerical method. The two previously known dynamo types lie in the same zone, and it is therefore possible to change the flow continuously from one to the other without losing dynamo action. Differential rotation is found to promote large-scale axisymmetric toroidal magnetic fields, while meridional circulation (M) promotes large-scale axisymmetric poloidal fields concentrated at high latitudes near the axis. Magnetic fields resembling that of the Earth are generated by $D > 0$, corresponding to westward flow at the surface, and M of either sign but not zero. Very few oscillatory solutions are found.

Keywords: kinematic dynamos; geomagnetism; eigenvalue problems

1. Introduction

The magnetic fields of stars and planets are generated by self-exciting dynamo action of electrically conducting fluid. In the Earth the dynamo resides in the molten iron outer core; in the Sun it resides at the base of the convection zone. Fluid flowing across magnetic field lines induces an EMF and corresponding magnetic field; given the right conditions and geometry, the induced magnetic field can reinforce existing ones, resulting in conversion of kinetic into magnetic energy. When the conversion is sufficiently strong, the dynamo self-excites and the original magnetic field

† Present address: School of Mathematical Sciences, University of Exeter, Exeter EX4 4QJ, UK.

Proc. R. Soc. Lond. A (2000) **456**, 1333–1353

© 2000 The Royal Society

1333

grows exponentially; dynamical forces then modify the flow until quasi-equilibrium is reached with either a steady state or fluctuations about an average field strength (see, for example, Moffatt 1978; Jacobs 1987; Proctor & Gilbert 1994; Proctor *et al.* 1993; Hollerbach 1996).

The kinematic dynamo problem addresses the question of how flows generate magnetic fields without consideration of the dynamical forces involved. The magnetic field is governed by Maxwell's equations in the non-relativistic limit and Ohm's law for a moving medium. These combine to give the induction equation, which governs the evolution of $\boldsymbol{B}$,

$$\frac{\partial \boldsymbol{B}}{\partial t} = R_{\mathrm{m}} \nabla \times (\boldsymbol{v} \times \boldsymbol{B}) + \nabla^2 \boldsymbol{B}, \tag{1.1}$$

where $\boldsymbol{v}$ is the fluid velocity, R_{m} the dimensionless magnetic Reynolds number

$$R_{\mathrm{m}} = \mathcal{V} L / \eta, \tag{1.2}$$

$\mathcal{V}$ the velocity scale, L the length-scale, and η the electrical diffusivity. Solutions are of the form $\boldsymbol{B} = \hat{\boldsymbol{B}} \exp{(\sigma + \mathrm{i}\omega)t}$, giving the eigenvalue equation

$$(\sigma + \mathrm{i}\omega)\hat{\boldsymbol{B}} = R_{\mathrm{m}} \nabla \times (\boldsymbol{v} \times \hat{\boldsymbol{B}}) + \nabla^2 \hat{\boldsymbol{B}}. \tag{1.3}$$

At the boundary, $\boldsymbol{B}$ matches to a potential field. Dynamo action is said to occur when a growing solution exists with $\sigma \geqslant 0$; the critical magnetic Reynolds number $R_{\mathrm{m}}^{\mathrm{c}}$ is the value corresponding to $\sigma = 0$.

Originally, investigators were concerned with whether dynamo action was possible (Elsasser 1946; Bullard & Gellman 1954). The first positive results were established analytically for idealized models (Herzenberg 1958; Backus 1958); later numerical calculations confirmed dynamo action in a sphere (Gubbins 1973; Kumar & Roberts 1975). Only recently has the subject developed sufficiently to study the relationship between the generated magnetic field and the underlying flow (Hutcheson & Gubbins 1994; Sarson & Gubbins 1996).

Until recently, the dynamics had been studied separately by isolating the effects of rotation and applied magnetic field on convection (see, for example, Busse 1970; Eltayeb & Kumar 1977; Moffatt 1970; Zhang & Busse 1989; Hollerbach & Jones 1993). Large-scale numerical simulations demonstrated dynamo action first in the solar (Gilman 1983) and then, more recently, in the geomagnetic (Glatzmaier & Roberts 1995; Kuang & Bloxham 1997) context. These fully dynamical calculations are so complex that a very limited range of parameters has been explored to date, and progress has been slow. In the case of the geodynamo, it is impossible to approach realistic parameter values, because the Earth's rotation is rapid and the diffusivities in the core are small. Kinematic studies can still contribute by defining those classes of flows that are capable of generating magnetic fields.

Numerical studies of kinematic dynamos have had an unhappy history, with early claims of dynamo action by Bullard & Gellman (1954) and Lilley (1970) later proving to be incorrect. We cannot rule out dynamo action on the basis of numerical results alone, we can only assert that a flow does not generate a magnetic field with the length- and time-scales resolved by the calculation. Numerical approximations that appear reasonable at low resolution can be qualitatively, not just quantitatively, misleading. The kinematic dynamo problem seems to be quite unusual in this respect:
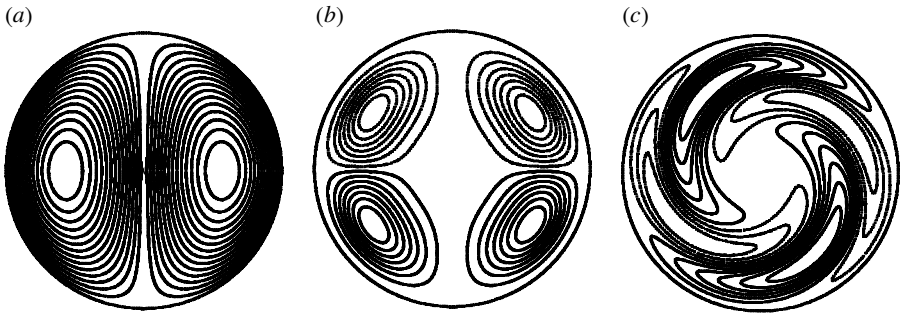
(a)   (b)   (c)

Figure 1. Fluid flow defined by equations (2.1)–(2.4). (a) Contours of v_ϕ, controlled by parameter ϵ_0, in meridian section. (b) Streamlines of meridional circulation (ϵ_1) in meridian section. (c) Streamlines of convection rolls (ϵ_2, ϵ_3) in equatorial section.

close inspection of most problems reveals spurious numerical solutions to be physically unreasonable. Some examples of deceptive, bogus solutions are given in the next section. We must therefore be careful with numerical convergence and cautious with interpretation. Our approach is to build confidence in the numerical solutions by linking them to known neighbouring analytical, asymptotic and well-established numerical solutions. Details are given in § 3.

How common is dynamo action by steady flow? There are two opposing views. The first argues by analogy with the mechanical dynamo, a complicated device that generates electric current and associated magnetic fields. Any homogeneous body of fluid doing the same job is expected to be similarly complicated, with a correspondingly intricate flow pattern: dynamo action might, therefore, be rare. The second view regards solutions of the induction equation as instabilities, which are ubiquitous in fluid-dynamical systems: dynamo action might, therefore, be very common. Anti-dynamo theorems prohibit dynamo action by some simple flows and numerical examples of dynamo action by flows in spheres have been remarkably difficult to find, both of which support the first view. On the other hand, asymptotic studies have revealed entire classes of flows that generate magnetic fields. Roberts (1972a) found that 'almost all' periodic flows in an infinite fluid generate magnetic fields, supporting the second view. In this paper we address this issue by defining a class of flows represented by just two parameters and determining the proportion that produce dynamo action.

2. The fluid flow

Kumar & Roberts (1975) studied the class of flows

$$\boldsymbol{v} = \epsilon_0 \boldsymbol{t}_1^0 + \epsilon_1 \boldsymbol{s}_2^0 + \epsilon_2 \boldsymbol{s}_2^{2c} + \epsilon_3 \boldsymbol{s}_2^{2s}, \tag{2.1}$$

where $\boldsymbol{t}_l^m$, $\boldsymbol{s}_l^m$ are toroidal and poloidal vector spherical harmonics,

$$\boldsymbol{t}_l^{m\left\{{\cos \atop \sin}\right\}} = \nabla \times \left[t_l^m(r) P_l^m(\cos\theta) \left\{{\cos \atop \sin}\right\}(m\phi)\boldsymbol{e}_r \right], \tag{2.2}$$

$$\boldsymbol{s}_l^{m\left\{{\cos \atop \sin}\right\}} = \nabla \times \nabla \times \left[s_l^m(r) P_l^m(\cos\theta) \left\{{\cos \atop \sin}\right\}(m\phi)\boldsymbol{e}_r \right], \tag{2.3}$$

where (r, θ, ϕ) are spherical coordinates, P_l^m are Schmidt-normalized associated Legendre functions, and $\boldsymbol{e}_r$ is the unit radial vector. The scalar functions were chosen to give a $\boldsymbol{v}$ that is differentiable at the origin, and to be zero with zero stress on the outer boundary:

$$\left.\begin{array}{l} t_1^0(r) = r^2(1 - r^2), \\ s_2^0(r) = r^6(1 - r^2)^3, \\ s_2^{2c}(r) = r^4(1 - r^2)^2 \cos(p\pi r), \\ s_2^{2s}(r) = r^4(1 - r^2)^2 \sin(p\pi r). \end{array}\right\} \tag{2.4}$$

The first harmonic represents differential rotation, the second meridional circulation, and the last two convective overturn; these three constituents of the flow are shown in figure 1. Kumar & Roberts (1975) developed this flow from simpler forms that failed to generate magnetic fields; in some sense they are the simplest flows that can generate the basic features of the Earth's magnetic field and mimic convection in a rotating sphere. Kumar & Roberts (1975) chose values of the parameters ϵ_i near the asymptotic regime studied by Braginsky (1964), the rather complicated limit $R_m \to \infty$ with $\epsilon_1 R_m$, $\epsilon_2 R_m^{1/2}$ and $\epsilon_3 R_m^{1/2}$ remaining finite. Subsequent studies (Nakajima & Kono 1991; Hutcheson & Gubbins 1994; Sarson & Gubbins 1996) also stayed in the Braginsky regime. Here, we fix $p = 3$ and $\epsilon_2 = \epsilon_3$, leaving a three-parameter flow defined by ϵ_0, ϵ_1 and R_m, and seek dynamo action away from the Braginsky regime.

Not all choices of the ϵ_i are independent because of symmetry. The transformations $\phi \to \phi + \pi/2$ and $\phi \to -\phi$ show the equivalence of the four combinations:

$$\begin{pmatrix} \epsilon_0 & \epsilon_1 & \epsilon_2 & \epsilon_3 \end{pmatrix},$$
$$\begin{pmatrix} \epsilon_0 & \epsilon_1 & -\epsilon_2 & -\epsilon_3 \end{pmatrix},$$
$$\begin{pmatrix} -\epsilon_0 & \epsilon_1 & -\epsilon_2 & \epsilon_3 \end{pmatrix},$$
$$\begin{pmatrix} -\epsilon_0 & \epsilon_1 & \epsilon_2 & -\epsilon_3 \end{pmatrix}$$

(see Dudley & James 1989). Our choice of $\epsilon_2 = \epsilon_3$ is, therefore, equivalent to $\epsilon_2 = -\epsilon_3$. Changing the sign of R_m reverses the flow, so the second of these combines with $R_m \to -R_m$ to produce the combination $\begin{pmatrix} -\epsilon_0 & -\epsilon_1 & \epsilon_2 & \epsilon_3 \end{pmatrix}$. Having set $\epsilon_2 = \epsilon_3$, we can therefore restrict R_m to positive values and still explore the full range of dynamo solutions defined by the two parameters ϵ_0 and ϵ_1.

We define R_m so that the total kinetic energy of the flow is unity:

$$\int v^2 \, \mathrm{d}V = \alpha\epsilon_0^2 + \beta\epsilon_1^2 + \gamma\epsilon_2^2 + \delta\epsilon_3^2 = 1, \tag{2.5}$$

where the scalars α, β, γ, δ are integrals of the radial functions (2.4). The fraction of energy in the meridional circulation is then

$$M = \mathrm{sgn}(\epsilon_1)\beta\epsilon_1^2, \tag{2.6}$$

and that for differential rotation

$$D = \mathrm{sgn}(\epsilon_0)\alpha\epsilon_0^2. \tag{2.7}$$

The remaining energy lies in convection

$$C = 1 - |M| - |D|. \tag{2.8}$$

The entire class of flows is defined by the diamond $|M| + |D| \leqslant 1$ (figure 4a). We search for dynamo action with $R_{\mathrm{m}}^{\mathrm{c}} > 0$. The differential rotation is zero at the surface and eastward within the sphere for $D > 0$; in the co-rotating frame with zero angular momentum, the surface flow would, therefore, be westward, as it is at the surface of the Earth's core (Kumar & Roberts 1975). $M > 0$ gives surface flow towards the Equator and away from the poles.

Four different solutions for $\boldsymbol{B}$ separate because of symmetries in the flow and the induction equation; they are either symmetric or antisymmetric under reflection in the equatorial plane or rotation through an angle π about the coordinate axis. They are linearly independent for the kinematic dynamo problem, but also separate for the fully dynamical dynamo problem (Gubbins & Zhang 1993). In this paper we restrict ourselves to the geophysically realistic 'dipole' symmetry (poloidal fields antisymmetric about the Equator), and to the simplest case of symmetry under rotation through an angle π about the coordinate axis. These solutions may not be the preferred mode, since other symmetries may have a lower critical magnetic Reynolds number. Results will be compared with solutions for the other three possible symmetries in a later paper.

Kumar & Roberts (1975) found solutions near the Braginsky limits $D \to \pm 1$, $M \to 0$, two corners of our diamond. Other solutions found subsequently by Hutcheson & Gubbins (1994) and Sarson & Gubbins (1996) also lie in the Braginsky regime. The axisymmetric field generated by these dynamos, $\bar{\boldsymbol{B}}$, satisfies the mean field equation

$$\frac{\partial \bar{\boldsymbol{B}}}{\partial t} = \nabla \times (\omega \boldsymbol{v}_{\mathrm{T}} \times \bar{\boldsymbol{B}}) + \nabla \times (\boldsymbol{v}_{\mathrm{e}M} \times \bar{\boldsymbol{B}}) + \nabla \times (\alpha \bar{\boldsymbol{B}}) + \eta \nabla^2 \bar{\boldsymbol{B}}, \qquad (2.9)$$

where $\boldsymbol{\omega}$ is the scale of differential rotation $\boldsymbol{v}_{\mathrm{T}}$, α depends on the helicity of the non-axisymmetric flow, and $\boldsymbol{v}_{\mathrm{e}M}$ is the meridional circulation plus an 'effective' part also depending on the non-axisymmetric flow (see, for example, Kumar & Roberts 1975; Sarson & Gubbins 1996). With our choice of $\{\epsilon_i\}$, the point $D = 1$ corresponds to $\alpha\omega < 0$, and the point $D = -1$ corresponds to $\alpha\omega > 0$. Solutions of these mean-field equations are usually referred to as $\alpha\omega$ dynamos; when $\omega = 0$ they are α^2 dynamos.

Love & Gubbins (1996) demonstrated dynamo action for flows with no differential rotation. These are plotted on the M-axis in figure 4a, between the approximate extremes $D = 0.00$, $M = -0.64$ and $D = 0.00$, $M = -0.02$. The generated fields were steady. The helicity of the flow, $\boldsymbol{v} \cdot \nabla \times \boldsymbol{v}$, is important for dynamo action (Moffatt 1978). These flows have an axisymmetric component of helicity and a non-axisymmetric component proportional to $\cos 2\phi$:

$$h = H_0(D, M) + H_1(D, M) \cos 2\phi. \qquad (2.10)$$

Surprisingly, no dynamo action was found at $(0.0, 0.0)$, where the flow is pure convection with optimal helicity (although we now know that the equatorial dipole symmetry is supported; see Holme (1997)). An α^2 dynamo might have been expected to operate but does not: in fact, the smallest scaled critical magnetic Reynolds number, and, therefore, in some sense the most efficient dynamo, occurred near the point with maximum non-axisymmetric helicity (Love & Gubbins 1996).

The boundary $|D| + |M| = 1$ has no convection and the flow is purely axisymmetric. Solutions of (1.1) separate into modes proportional to $\exp im\phi$; there is no dynamo action with $m = 0$ because of Cowling's theorem: no axisymmetric magnetic field can be sustained. Holme (1997) has searched for dynamos with $m = 1$ without success

Table 1. *Critical magnetic Reynolds number for a flow with $D = +0.50$, $M = -0.08$*

(The extrapolation has converged to four significant figures by $L = 24$.)

n_r	50	100	150	extrapolated
$L = 8$	128.59	129.85	130.09	130.28
10	127.99	129.92	130.27	130.56
12	128.44	129.99	130.28	130.52
14	129.14	130.98	131.33	131.61
16	128.48	130.14	130.44	130.69
18	128.99	130.75	131.08	131.35
20	128.70	130.40	130.72	130.97
22	128.86	130.59		131.17
24	128.78	130.50		131.07
26	128.82	130.54		131.12
28	128.81	130.54		131.11
30	128.83	130.56		131.14

(although he did find some with modified radial functions). Further solutions with this symmetry will be described in a later paper.

Existing knowledge of dynamo action by this class of flows is, therefore, restricted, despite a great deal of effort over several decades, to small patches near the two corners $D = \pm 1$ and a line on the $D = 0$ axis. In this paper we attempt to explore the diamond and discover how much of it defines flows that generate magnetic field with dipole symmetry. Numerical difficulties will prevent us from achieving this goal fully, so these are discussed first.

3. Numerical considerations

Equation (1.3) is solved by the method first developed by Bullard & Gellman (1954), described there with extensions in Gubbins (1973), Hutcheson & Gubbins (1994) and Sarson & Gubbins (1996). $\hat{\boldsymbol{B}}$ is expanded in vector spherical harmonics to a maximum degree L, and radial derivatives are represented by second-order finite differences with n_r points. This converts the partial differential equation to an algebraic eigenvalue equation, which can be solved by a number of standard methods (Golub & Van Loan 1989). We either fix R_m and solve for the growth rate $\sigma + i\omega$ as eigenvalue, or assume a steady solution and solve the generalized eigenvalue problem for the critical magnetic Reynolds number R_m^c. The first method is useful because we depart from known, decaying, analytical solutions at $R_m = 0$ and gradually increase R_m until a steady or growing solution is found, giving a growth rate curve. The second method is useful for refining a known or suspected steady solution.

The QR algorithm gives all the eigenvalues reliably but requires a great deal of memory: it is impractical for the larger calculations reported here. Inverse iteration finds the eigenvalue closest to a chosen starting value, takes advantage of the banded structure of the matrix, and requires much less computer memory. We are usually only interested in the solution with smallest R_m^c, because the others are not physically realizable; inverse iteration is ideal for refining this one eigenvalue when it is clearly distinguishable from others. It does not work well when there are several similar

Table 2. $D = -0.50$, $M = -0.20$ *convergence table for steady solutions*

n_r	25	50	100	extrapolated
$L = 6$	151.78	167.13	170.28	171.27
8	153.96	167.61	170.67	171.66
10	*	*	—	*
12	—	232.97	239.06	241.09
14	—	340.79	353.40	357.60
16	245.11	286.52	292.09	293.52
18	—	*	*	*
20	—	352.29	360.88	363.74
22	—	619.55	672.35	689.95
24	—	421.03	435.24	439.98
26	—	*	*	*

*No solution was found.
—No solution was sought.

eigenvalues, or for tracing jumps from one eigenvalue to another (with change of resolution for example, cf. tables 2 and 3). The most effective method is the implicitly restarted Arnoldi method (IRAM), which finds the k eigenvalues closest to a chosen starting value, where k is chosen to suit the problem (10 in our case) (Lehoucq *et al.* 1998; Arnoldi 1951; Sorensen 1992). A suite of growth rates for R_m increasing from zero to the critical value helps identify cross-overs and conversions of real to complex eigenvalues.

Convergence of the algebraic solution is checked by increasing the L and n_r and comparing solutions. It is sometimes helpful to refine the eigenvalue by Richardson extrapolation on n_r, the number of radial points. Weak dependence of the eigenvalue on truncation can mask poor convergence, and it is advisable to inspect the eigenfunctions, either by comparing solutions at different truncations or by examining the spectrum for peaks at high spherical harmonic degree.

Numerical convergence is critical to the success of these calculations; some examples are given here to explain and justify the procedures used later. Table 1 shows a reasonably well-converged solution (by no means the best example). The spectrum of energy by spherical harmonic degree is shown in figure 2; it drops off smoothly with less than 1% of the energy being contained above degree 12. Most importantly, the lower harmonics do not change significantly when the truncation is raised. Inspection of the radial functions for each harmonic also shows little change at higher truncation.

Table 2 shows a convergence failure. The agreement between $L = 6$ and $L = 8$ is quite encouraging. Early studies were restricted to similar truncations: Bullard & Gellman (1954) stopped at $L = 4$; Lilley (1970) at $L = 6$; and Kumar & Roberts (1975) at $L = 10$. The corresponding eigenvectors (figure 3) do not agree so well. Even this warning does not prepare us for the divergence to follow at higher truncation (table 2). This kind of behaviour deceived both Bullard & Gellman (1954) and Lilley (1970), who were restricted to low truncation and claimed solutions that were later discovered to be bogus.

Table 3 shows a different eigenvalue for the same flow. Roberts (1972b) discusses the numerical problems associated with rapidly oscillating solutions and requires that
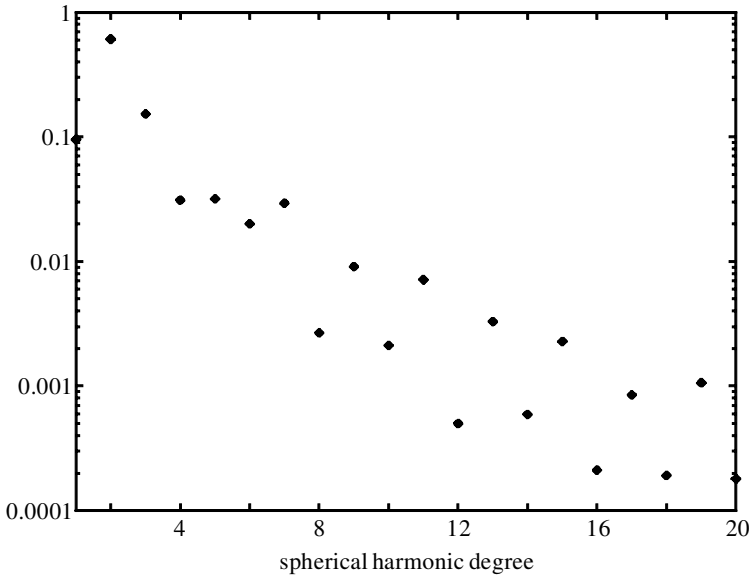
Figure 2. Decrease of energy with spherical harmonic degree for the dynamo with $D = 0.50$, $M = -0.08$. The rapid fall-off is indicative of good numerical convergence.
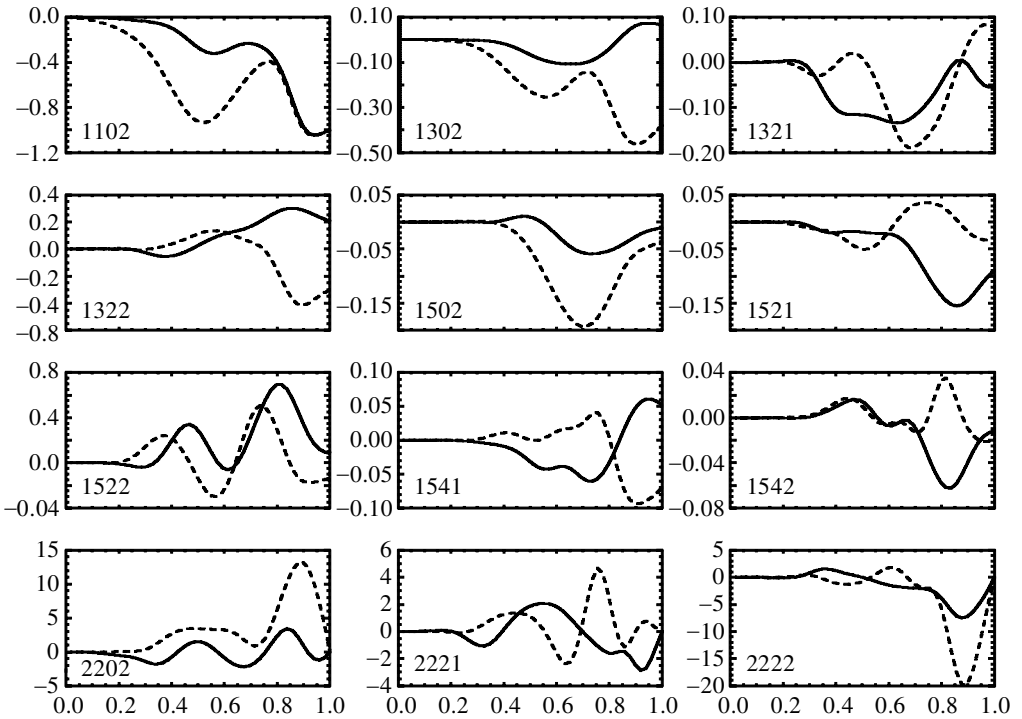

Figure 3. Comparison of eigenvectors for two different truncations $(L = 6, 8)$ for the dynamo with $D = -0.50$, $M = -0.20$. The agreement is poor, whereas R_m^c appears converged at this level (table 2).

Table 3. $D = -0.50$, $M = -0.20$ *convergence table for oscillatory solution*

(Figures in brackets are the imaginary part of the growth rate.)

n_r	25	50	100	extrapolated
$L = 6$	156.4 (130)	162.3 (128)	163.9 (127)	164.4 (127)
8	* (—)	292.0 (208)	295.2 (214)	296.3 (216)
10	184.2 (135)	195.3 (143)	— (—)	199.1 (146)
12	— (—)	* (*)	* (*)	* (*)
14	— (—)	231.5 (165)	235.9 (169)	237.4 (170)
16	261.4 (190)	257.4 (191)	259.0 (193)	259.8 (194)
18	— (—)	245.1 (173)	248.3 (180)	249.4 (182)
20	— (—)	252.2 (186)	254.2 (188)	254.9 (189)
22	— (—)	247.9 (180)	250.2 (181)	251.0 (181)
24	— (—)	249.5 (183)	251.8 (185)	252.6 (186)
26	— (—)	248.7 (181)	251.0 (184)	251.8 (185)

Table 4. *Convergence table for steady solution at* $D = -0.45$, $M = -0.40$

n_r	50	100	150	extrapolated
$L = 6$	93.1	—	—	93.1
8	113.0	—	—	113.0
10	139.6	—	—	139.6
12	178.1	182.6	—	184.1
14	*	*	—	*
16	176.7	180.1	—	181.2
18	182.3	184.5	—	185.2
20	178.2	181.3	181.8	182.3
22	180.3	182.9	183.4	183.8
24	178.4	181.2	181.8	182.2
26	179.9	182.6	183.1	183.5

the electromagnetic skin depth be resolved, or $\Delta x < \sqrt{1/\omega}$, where Δx is the spatial resolution. In our case, solutions with ω less than 400 should be well resolved. The solution is variable at low truncation and sometimes disappears (notably at $L = 12$), probably because of the large ω, but it settles down after $L = 14$ and $n_r = 50$. A neighbouring flow produces a well-converged steady dynamo (table 4). Like the oscillatory solution in table 3, there is little evidence of converged dynamo action at low truncation.

Lack of dynamo action at low truncation is probably caused by failure to resolve small-scale fields that play an essential part in the regeneration process. Other solutions have R_m^c values that oscillate, sometimes wildly, as the truncation point is increased. This is usually indicative of a small-scale solution with a particular symmetry that requires only certain harmonics for its description.

Numerical difficulties and abrupt changes of the dynamo action with small changes in velocity led to the following strategy.

(1) Compute growth rate curves by Arnoldi iteration for all flows on a (D, M) grid with 0.05 spacing using a low truncation (we used $L = 12$, $n_r = 50$).

(2) Repeat at a higher truncation ($L = 18$, $n_r = 50$).

(3) Use inverse iteration to study further those calculations yielding values of R_m^c that differ by less than 20% at the two truncations.

(4) Discard those flows whose R_m^c fail to converge to at least two significant figures.

(5) Study the generated magnetic field (eigensolution); this should not change significantly at different truncations. Some solutions were rejected by this criterion.

(6) Further calculations were needed on a finer (D, M) grid in places where dynamo action changed rapidly.

4. Steady dynamos

In figure 4a we show the scaled R_m^c in (D, M)-space for steady solutions with dipole symmetry. The different zones, labelled A–G, are separated by regions in which no dynamos have been found. The boundaries of the zones are characterized by rapidly increasing R_m^c and poor numerical convergence. There are also some isolated oscillatory solutions within the zones, which are the subject of an ongoing study.

R_m^c increases with $|D|$, approaching infinity in the Braginsky limit, and generally decreases as $|M|$ increases from zero (the minimum is reached within zone A along a line approximately following the solutions in table 5). A flow with small R_m^c can generate magnetic field with less kinetic energy than one with a larger R_m^c; R_m^c, therefore, represents one measure of the 'efficiency' of the flow in generating magnetic field.

Figure 4b shows the non-axisymmetric part of the helicity, H_1 in (2.10). Love & Gubbins (1996) showed that the non-axisymmetric part produced a lower R_m^c for the poloidal-only flow dynamo (along the axis $D = 0$, and this figure shows that the same situation holds in the more general case with differential rotation, at least in the largest zones A and C.

Another measure of efficiency is the ohmic heating divided by the magnetic energy,

$$O = \left(\frac{L}{\pi}\right)^2 \frac{\int (\nabla \times \boldsymbol{B})^2 \, dV}{\int \boldsymbol{B}^2 \, dV}, \tag{4.1}$$

where the integral is taken over the whole core. The factor (L/π^2) ensures $O \geqslant 1$, the optimum efficiency $O = 1$ being achieved when $\boldsymbol{B}$ is the fundamental dipole decay mode (Gubbins & Roberts 1987). This quantity gives the power required to sustain unit magnetic energy at the critical point. Figure 5a shows $O(D, M)$; the plot is similar to that of R_m^c,

Figure 5b shows the percentage of magnetic energy in the poloidal field. It is low for large $|D|$ because differential rotation generates large toroidal fields. At small $|D|$, large M, the field is over 90% poloidal. Figure 5c shows the percentage of energy
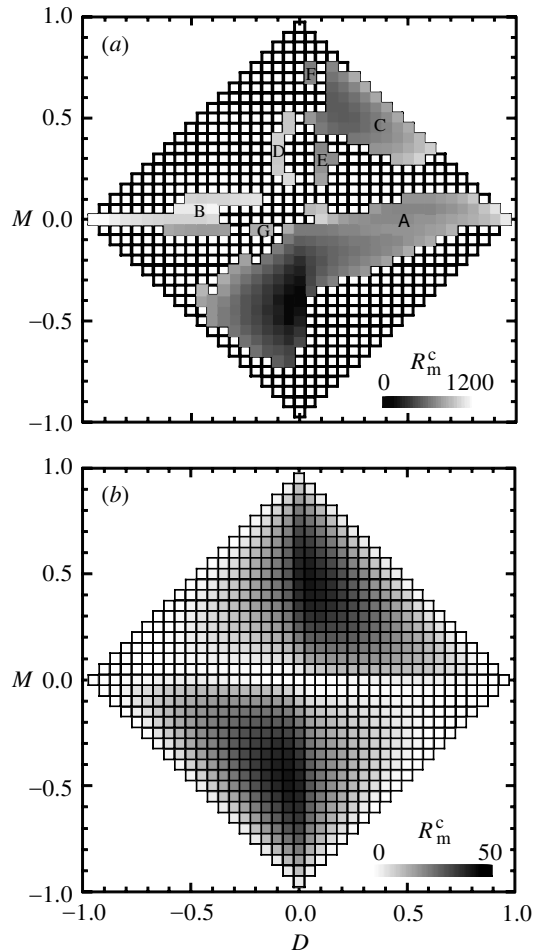
Figure 4. (*a*) Flows giving dynamo action. R_m^c as shown by the grey scale at the bottom right. (*b*) Non-axisymmetric helicity of the flow, $H_1(D, M)$ in (2.10). Note the correspondence with R_m^c, suggesting it promotes dynamo action.

in the axisymmetric part of the field, which tends to increase away from the centre ($D = 0$, $M = 0$): differential rotation promotes axisymmetric toroidal field, while meridional circulation promotes axisymmetric poloidal field. Figure 5*d* shows the percentage of poloidal energy that is in the axisymmetric part, which shows that differential rotation does not promote axisymmetric poloidal field. Dynamos near the Braginsky limits mainly have non-axisymmetric poloidal fields, in agreement with the Braginsky scaling $B_T : B' : B_P = 1 : R_m^{-1/2} : R_m^{-1}$, where B_T is the toroidal field strength, B' the non-axisymmetric field, and B_P the axisymmetric meridional field.

The preceding results establish that a substantial proportion of the flows generate magnetic fields—*ca.* 36% of the squares in figure 4*a* are covered. However, in some areas, solutions change character or disappear for very small changes of D or M, necessitating a finer grid. We therefore carefully established dynamo action along a line in (D, M)-space joining the two previously known solutions: the Braginsky limit

Table 5. *Properties of solutions along a line joining the purely poloidal flow dynamos of*
Love & Gubbins (1996) and the Braginsky limit point $(1, 0)$

('O' is ohmic heating/energy (equation (4.1)); 'ohmic' is ohmic heating scaled to Earth $\times 10^7$ W;
'% axi' is percentage energy in the axisymmetric component of the field; '% P' in the poloidal
field; '% axiP' in the poloidal part of the field; '$P_{\max}$' is the dominant poloidal harmonic; '$T_{\max}$'
the dominant toroidal harmonic.)

D	M	R^c_m	O	ohmic	% axi	% P	% axiP	$P_{\max}$	$T_{\max}$
0.00	-0.36	44.01	84.0	2.8	79.2	76.5	90.1	3 0	2 0
0.05	-0.26	54.96	91.9	3.7	76.1	70.1	84.2	3 0	2 0
0.10	-0.20	64.34	96.2	4.4	74.4	63.6	79.5	1 0	2 0
0.15	-0.17	72.75	99.7	5.2	73.7	58.6	76.3	1 0	2 0
0.20	-0.15	80.17	101.0	6.0	73.5	54.3	73.8	1 0	2 0
0.25	-0.14	86.97	103.0	6.8	73.4	51.3	71.8	1 0	2 0
0.30	-0.13	93.59	103.0	7.7	73.6	48.2	69.9	1 0	2 0
0.35	-0.12	100.67	102.0	8.5	74.0	45.0	67.9	1 0	2 0
0.40	-0.11	108.53	102.0	9.6	74.4	41.8	66.0	1 0	2 0
0.45	-0.10	117.70	100.0	10.8	75.0	38.5	64.1	1 0	2 0
0.50	-0.08	128.69	95.5	11.8	76.7	33.3	61.2	1 0	2 0
0.55	-0.07	141.57	93.5	13.5	77.7	30.1	59.0	1 0	2 0
0.60	-0.05	157.48	85.9	14.6	80.1	24.8	55.8	1 0	2 0
0.65	-0.04	175.52	82.1	16.9	81.7	21.6	53.1	1 0	2 0
0.70	-0.03	197.81	77.5	19.8	83.6	18.2	50.3	3 2	2 0
0.75	-0.02	226.00	71.8	23.5	85.9	14.8	47.4	3 2	2 0
0.80	-0.01	265.75	64.8	28.4	88.9	11.1	45.3	3 2	2 0
0.85	0.00	270.45	63.7	40.9	94.1	3.9	67.6	1 0	2 0
0.90	0.00	378.06	64.1	78.3	95.0	2.3	57.8	1 0	2 0
0.95	0.001	394.78	65.4	157.0	97.6	2.1	58.3	1 0	2 0
0.99	0.0001	1318.76	59.1	1570.0	99.3	0.4	23.7	3 2	2 0

($D = 1$, $M = 0$) and the poloidal-only dynamos ($D = 0$, $M < 0$). The results are
shown in table 5. This line serves two purposes: it establishes, as far as is possible
in a numerical study, continuity of dynamo action over a continuous range of D and
M, and it verifies numerical convergence at very high resolution for some of the
solutions.

The line roughly follows the minimum in R^c_m (figure 4a); these dynamos have
the best numerical convergence. Starting with the solution closest to the Braginsky
limit, $D = 0.99$, $M = 0.0001$, R^c_m is large and most of the energy is concentrated
in the toroidal field. The largest toroidal harmonic is T^0_2, as it is for all solutions
along this line, which is generated by the dominant differential rotation. The largest
poloidal harmonic is S^2_3, a part of the non-axisymmetric field B'. This solution is,
therefore, consistent with the Braginsky limit, as shown by Hutcheson & Gubbins
(1994).

The next solution, $D = 0.95$, $M = 0.001$, is also dominated by the axisymmetric
toroidal field, but now the largest poloidal harmonic is the axial dipole, and slightly
over half the poloidal energy is in the axisymmetric field. Strictly speaking, this is
out of the Braginsky regime, because the asymptotic scaling requires the poloidal
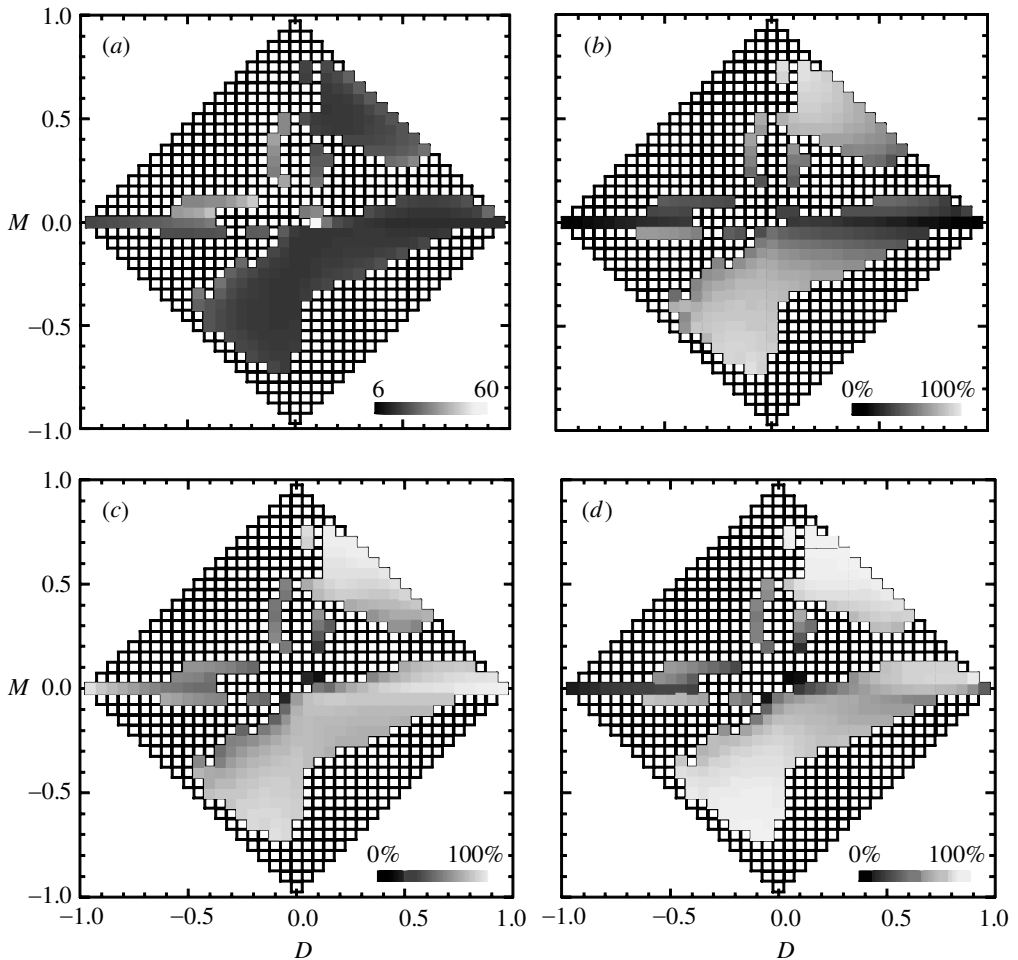field to be predominantly non-axisymmetric.

Figure 5. Physical properties of solutions. (*a*) Ohmic heating divided by magnetic energy, O in equation (4.1). (*b*) Percentage energy in the poloidal field. (*c*) Percentage energy in the axisymmetric part of the field. (*d*) Percentage of poloidal energy that is axisymmetric.

Proceeding along the line, we see a monotonic decrease in critical magnetic Reynolds number from $D = 0.99$ to $D = 0$. In some sense, this means that the Braginsky dynamo is the least efficient, because it requires the most kinetic energy to achieve dynamo action. However, O is a maximum at $D = 0.25$ and decreases to a minimum at the Braginsky limit. In this sense, the Braginsky limit is the most efficient dynamo, reflecting the dominance of the low-order toroidal harmonic T_2^0, which contributes relatively little to O. Scaling up the ohmic heating to geophysical values by matching the axial dipole to its 1980 value of $-30\,000$ nT gives an estimate in watts (column 5). This energy also shows a monotonic increase towards the Braginsky limit. All these values could be accommodated within the heat budget of the core (see, for example, Labrosse *et al.* 1997).

For all the dynamos found here, most of the magnetic energy resides in the axisymmetric part of the field, with a minimum at $D = 0.25$ rising towards the Bragin-
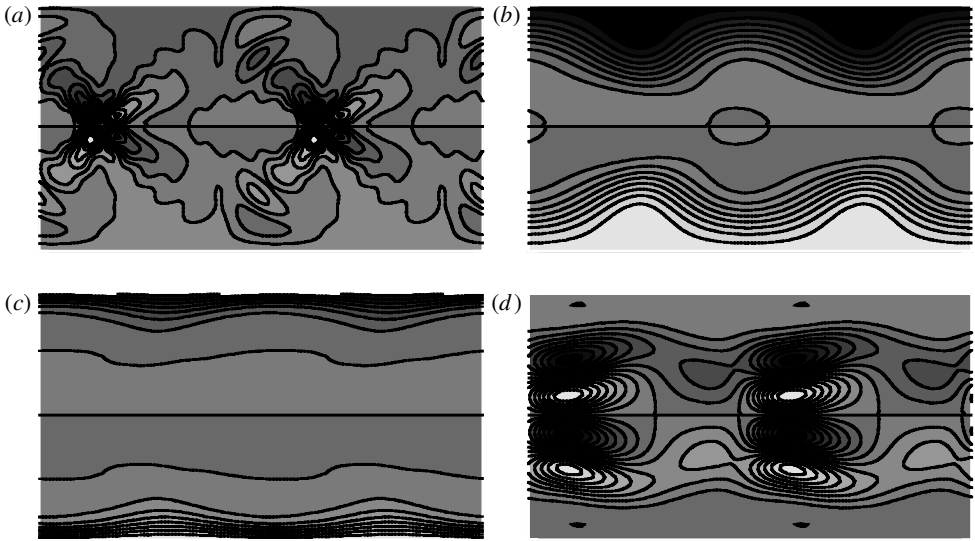
Figure 6. B_r at surface. (*a*) $D = -0.50$, $M = 0.10$ ($R_m^c = 484$). (*b*) $D = 0.95$, $M = 0.00$ ($R_m^c = 727$). (*c*) $D = 0.65$, $M = -0.05$ ($R_m^c = 179$). (*d*) $D = -0.95$, $M = 0.00$ ($R_m^c = 2141$).

sky asymptotic limit of 100% (column 5). However, the percentage of axisymmetric energy in the poloidal field falls monotonically with increasing D towards the Braginsky limit.

5. The generated fields

The morphology of the generated magnetic fields holds clues about how the dynamo operates. The surface field is important because it is all we can observe: we therefore discuss this first and then relate it to the internal field.

(*a*) *Surface field, B_r*

The existence of distinct zones separated by gaps in figure 4*a* with no apparent dynamo action is surprising. Even more surprisingly, the field morphology varies considerably within some zones but does not always change much between adjacent zones. For example, within zone A, the fields near the centre are quite different from those with large positive D, which are quite similar to those in zone C.

All solutions near the centre of the diamond, irrespective of zone, have surface field concentrated into small patches on the Equator, producing a pattern like two four-leaf clovers (figure 6*a*). The absence of any dynamo at the very centre, $D = M = 0$, is attributed to this small scale: its high diffusion can only be overcome by large R_m, which, in turn, produces smaller scales. The clover-leaf pattern is quite different from the surface field found near the Braginsky limit, which is closer to an axial dipole structure (figure 6*b*).

The dependence of the surface field on D and M is best described in terms of the separate effects of differential rotation and meridional circulation on the field generated near the centre of the diamond (small $|D|$ and $|M|$, figure 4*a*). Meridional circulation promotes large-scale fields with flux concentrated towards the poles. The
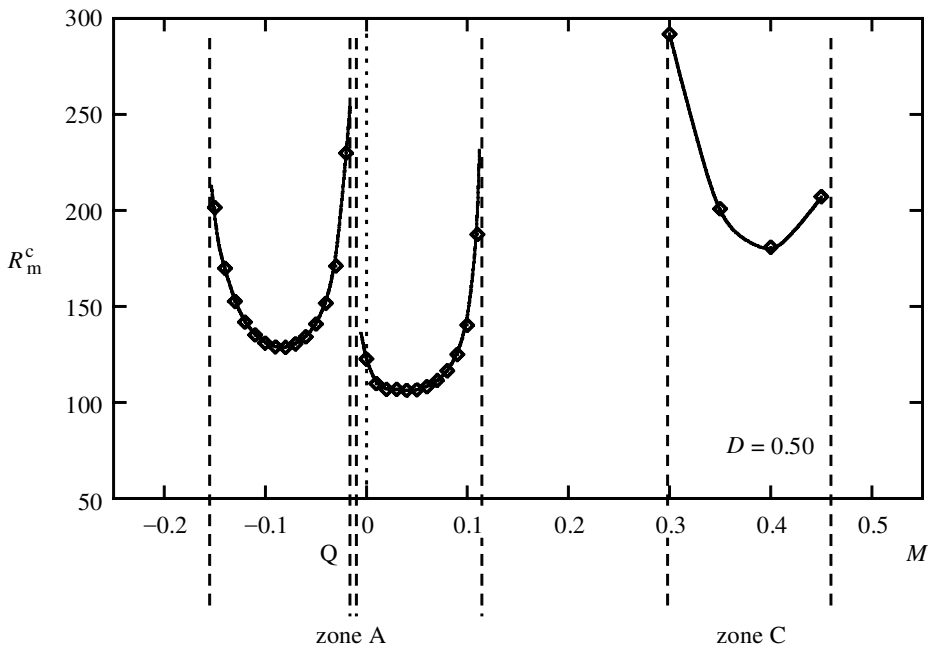
Figure 7. A section through figure $4a$ for $D = 0.50$. $R_{\mathrm{m}}^{\mathrm{c}}$ increases dramatically at the edges of the zones where dynamo action fails. At point Q an oscillatory solution is preferred.

clover-leaf pattern continues near the upper edge of zone A ($M > 0$). Near the Braginsky limit the flux lies mainly at the poles, with some residual evidence of the equatorial clover-leaf pattern ($D = 0.95$, $M = 0.00$, figure $6b$). As M decreases within zone A, the polar flux dominates completely ($D = 0.65$, $M = -0.05$, figure $6c$). The same happens in zone B, with an equatorial clover-leaf pattern near the upper edge and large-scale fields similar to those in figure $6b$ on the lower edge.

Differential rotation tends to elongate the features in longitude. Its effect is less dramatic than that of M. Increasing $|D|$ stretches the small flux concentrations of the clover-leaf pattern and pulls one pair above the other, as in figure $6d$ for $D = -0.95$, $M = 0.00$. This is close to a Braginsky limit and again reflects the Braginsky scaling, with a dominant non-axisymmetric poloidal magnetic field. A small amount of meridional circulation is enough to promote axial symmetry in both zones A and B.

The small zones D, E and G have the clover-leaf equatorial pattern, while zone F, with its larger $|M|$, has a large-scale pattern similar to that in figure $6b$. The other large zone, C, has the clover-leaf equatorial structure and some polar flux near its lower edge. Increasing M moves flux to the poles again to form a pattern similar to figure $6b$. Surface fields throughout the central part of zone C are very similar.

The effect of negative M on zones A and B can be attributed to surface flow sweeping flux towards the poles. However, this mechanism cannot explain the behaviour in zones C and F, where flux still concentrates towards the poles, even though the surface flow is towards the Equator. This behaviour can only be understood in connection with the morphology of the internal field.
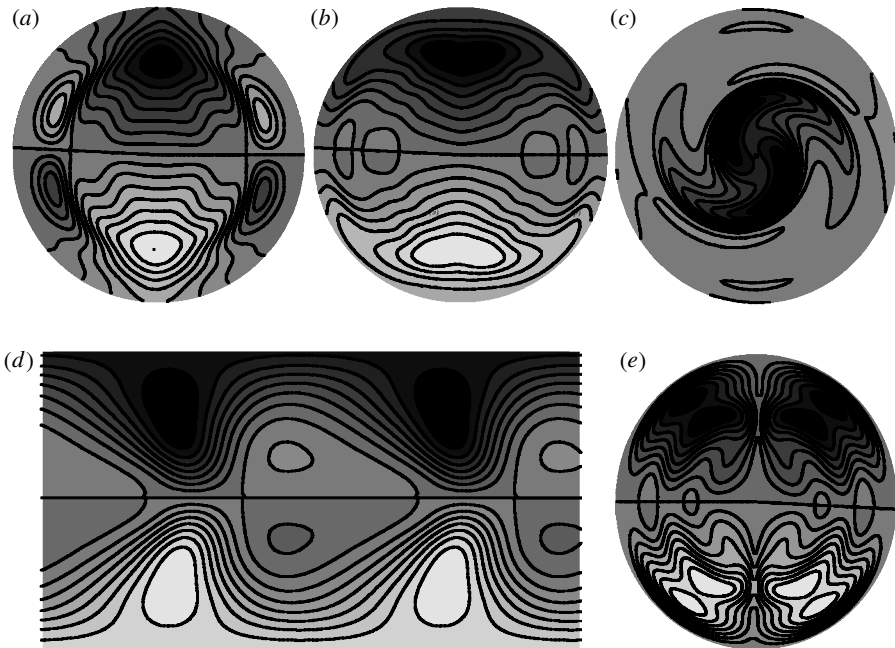
Figure 8. Magnetic field for $D = 0.65$, $M = 0.00$ ($R_{\mathrm{m}}^{\mathrm{c}} = 152$) in zone A. (*a*) B_r in meridian section, $\phi = 0°$. (*b*) B_r in meridian section, $\phi = 90°$. (*c*) B_θ in equatorial section. (*d*) B_r on surface. (*e*) B_ϕ in meridian section, $\phi = 0°$.

Figure 7 illustrates the change in $R_{\mathrm{m}}^{\mathrm{c}}$ across the boundaries of the zones. This graph corresponds to a section $D = 0.50$ in figure 4*a*. $R_{\mathrm{m}}^{\mathrm{c}}$ rises sharply at the boundaries of zones A and C, and also near $M \approx -0.01$, where an oscillatory solution appears. These oscillatory solutions will be discussed in part III of this series of papers. The rise in $R_{\mathrm{m}}^{\mathrm{c}}$ at the boundaries is usually accompanied by generation of small-scale field. The lower boundary of zone A has flux concentrated near the poles (cf. figure 6*c*), and dynamo action probably fails for $M < -0.16$ because flux is expelled from the dynamo region by the meridional circulation. The upper boundary of zone A has flux concentrated on the Equator, similar to that in figure 6*a* but extended laterally by the differential rotation. The boundaries of zone C seem to be controlled by the effect of meridional circulation on the toroidal, rather than the poloidal, field. At the lower boundary, the toroidal field is concentrated on the Equator, while at the upper boundary there is an additional concentration in the outer part of the sphere.

(*b*) *Internal fields*

The morphology of the internal field does not depend critically on the zone, as was the case for the surface field. Both D and M tend to promote large-scale field. The convective part of the fluid flow has three radial cells (cf. equations (2.4)). This structure is reflected in cellular magnetic fields near the centre of the diamond.

Figure 8 shows the internal field for $D = 0.65$, $M = 0.00$ in zone A. B_r is strongest along the axis and changes sign away from the axis near the Equator (figure 8*a,b*). The plot of B_θ in the equatorial plane shows departures from axial symmetry as
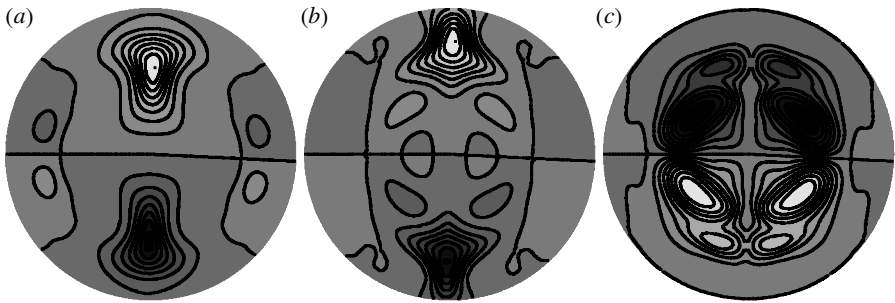
Figure 9. Magnetic field for dynamos with $D = 0.65$ in zone A. (a) B_r in meridian section, $M = -0.05$ ($R_m^c = 179$). (b) Same for $M = 0.05$ ($R_m^c = 122$). (c) B_ϕ in meridian section, $\phi = 0$, $M = -0.05$.
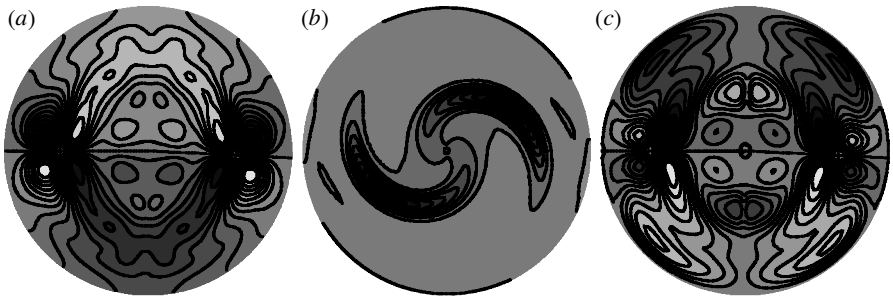

Figure 10. Magnetic field for $D = 0.20$, $M = 0.00$ ($R_m^c = 156$) in zone A. (a) B_r in meridian section. (b) B_θ in equatorial section. (c) B_ϕ in meridian section, $\phi = 0$.

well as axial concentration of the entire poloidal field. The surface field is also non-axisymmetric; the lower-latitude flux on longitudes $\pm 90°$ in figure 8b correspond to the equatorial features in the surface field, figure 8d. The azimuthal field is concentrated in high latitudes; it is mainly large scale, but there is some evidence of the underlying three-cell structure of the flow (figure 8e).

Increasing D from 0.65 towards the Braginsky limit $D = 1$ concentrates the flux towards the axis and the poles. The axially symmetric field dominates and the three-cell structure is lost. Changing M from zero concentrates the poloidal field onto the axis, the shape of the maximum flux regions reflecting the sign of M (figure 9a,b). The toroidal field for $M < 0$ is concentrated at mid-radius (figure 9c) and in the outer part of the sphere for $M > 0$ (not shown); it reflects something of the three-cell flow structure at all values of M.

The three-cell structure is more apparent for smaller D. Figure 10 shows the field for $D = 0.20$, $M = 0.00$ in zone A. When $D < 0$ in zone A, the field is also cellular and the toroidal field is concentrated towards the Equator. The same is true in zone B.

In zone C the poloidal field is mainly concentrated along the axis, while the toroidal field is cellular. When M is small within this region, for example at $D = 0.05$, $M = 0.50$, the toroidal field is again concentrated at the Equator; associated weak poloidal flux comes to the surface to form the clover-leaf pattern seen in many dynamos near the centre of the diamond. When M dominates (e.g. at $D = 0.25$, $M = 0.55$), it

seems that downwelling at the Equator depresses this flux to leave a surface field dominated by polar flux.

Zones D, E and G have small-scale cellular fields similar to those in zone A with small D and M. Zone F has axial poloidal field and cellular toroidal field, similar to neighbouring dynamos in zone C.

(*c*) *Interpretation*

Dynamos toward the centre of the diamond all generate small-scale magnetic fields that reflect the three-cell structure of the flow, the surface field is concentrated at the Equator over the downwelling parts of the flow, and toroidal and poloidal fields have comparable energy. This points to an α^2 mechanism working from two length-scales. Normally, two-scale dynamos are dominated by the large-scale field (Moffatt 1978), but here the ratio of length-scales is not that small (1/3) and the small-scale field is significant.

Differential rotation generates toroidal field. For $D \to 1$, the toroidal field is large scale and does not have the cellular structure. This points to an $\alpha\omega$ mean-field mechanism, with differential rotation generating $\boldsymbol{B}_{\mathrm{T}}$ from the large scale poloidal field. For $D < 0$, $\boldsymbol{B}_{\mathrm{T}}$ remains cellular until $D \approx -0.95$.

For large, positive M, $\boldsymbol{B}_{\mathrm{P}}$ is concentrated along the axis, while $\boldsymbol{B}_{\mathrm{T}}$ takes on a cellular structure. These dynamos do not have an analogue in the mean-field or Braginsky approximations, but it appears that $\boldsymbol{B}_{\mathrm{T}}$ continues to be generated from poloidal field by the convection, while large-scale $\boldsymbol{B}_{\mathrm{P}}$ is generated by the meridional circulation from $\boldsymbol{B}_{\mathrm{T}}$. The same occurs when $M < 0$, but the shape of the region of concentrated poloidal flux is different.

6. Conclusions

A primary goal of this study was to establish whether dynamo action by steady flows is rare or common. We found that *ca.* 36% of our two-parameter family of flows generate magnetic fields with dipole symmetry. The precise figure depends on the parametrization; for example, it would be higher if M were restricted, as might be expected in rotating convection. However, the general conclusion is that rather few flows act as dynamos.

This study required a large number of numerical solutions of the induction equation. These were obtained by first exploring the 10 eigenvalues with largest real part using iteratively restarted Arnoldi iteration, then refining a single eigenvalue at high resolution using inverse iteration. IRAM represents a major step forward in the numerical methods used on the kinematic dynamo problem.

The flows include two types of dynamo that were known from previous studies, the Braginsky limit of Kumar & Roberts (1975) and the poloidal flow dynamo of Love & Gubbins (1996). The first is dominated by differential rotation and produces a large toroidal field, while the second has no differential rotation and generates magnetic field through the azimuthal variation of helicity. We have established a line of dynamos joining the two; it is therefore possible to change one flow into the other in a continuous fashion without losing dynamo action. The smallest critical magnetic Reynolds number falls near the maximum non-axisymmetric helicity, as was found by Love & Gubbins (1996) for zero differential rotation, suggesting that azimuthal

variation of helicity assists magnetic field generation for all dynamos away from the Braginsky limit.

Dynamo action occurs in discrete zones in velocity parameter space. They are separated by regions where no known dynamo action occurs, or at least no magnetic fields are generated that can be represented with the numerical resolution used. At the boundaries of these regions the critical magnetic Reynolds number rises dramatically and the generated field becomes small scale. The effect is so sharp that further increases in resolution are unlikely to yield many more solutions. Surprisingly, adjacent zones can generate quite similar magnetic fields, while the field can change dramatically with a small change in flow within one zone. The gaps in dynamo action between the zones are attributed to flows that concentrate flux into very small regions between the fluid cells, or at the boundaries where the magnetic energy is lost to the insulator. The effect might, therefore, be restricted to steady flows.

Almost all the solutions are steady, which is surprising because the majority of solutions to the mean field $\alpha\omega$ equations are oscillatory (Roberts 1972b). A small number of oscillatory solutions corresponding to the $\alpha\omega$ limit had already been found near the points $D = \pm 1$ (Sarson & Gubbins 1996); they continue along a fine line in (D, M) parameter space and at a small number of other isolated points. These time-dependent solutions will be examined in a separate study.

Dynamos with weak meridional circulation and differential rotation, near the centre of the parameter-space diamond, generate magnetic fields that are concentrated on the Equator with a double clover-leaf pattern at the surface. They appear to operate from an α^2 mechanism; the flux is often concentrated near longitudes $\pm 90°$, near the downwelling limbs of the convection. They are inefficient, with a large critical magnetic Reynolds number and ohmic heating:magnetic energy ratio, because the fields are small scale. Dynamo generation of the axial dipole symmetry fails altogether at the very centre of the diamond.

The morphology of generated fields elsewhere in the diamond can be understood in terms of the action of differential rotation and meridional circulation on this central clover-leaf pattern. Both promote larger scale fields. Differential rotation generates axisymmetric toroidal field and stretches out the poloidal field in longitude. For large D, the dynamo action changes from α^2 to $\alpha\omega$; the intermediate region cannot be described as either. The poloidal field in this intermediate region tends to show the underlying three-cell structure of the flow (cf. figure 8a, e), suggesting that it is partly generated by convective flow acting on the toroidal field. Similarly, the toroidal field exhibits some three-cell structure, suggesting it is generated by the convective flow (figure 8e, 9c).

At the Braginsky limits $D = \pm 1$, the poloidal field becomes dominated by its non-axisymmetric component. Dynamos with large M, $D \neq 0$ do not correspond to any known mean-field equation. Meridional circulation promotes large-scale axisymmetric poloidal field concentrated mainly along the axis. The toroidal field is weak and continues to show the underlying three-cell structure of the flow, suggesting that it is generated by the action of convection rather than differential rotation. Usually, the poloidal and toroidal fields occupy different physical regions of the sphere.

References

Arnoldi, W. E. 1951 The principle of minimized iterations in the solution of the matrix eigenvalue problem. *Q. J. Appl. Math.* **9**, 17–29.

Backus, G. E. 1958 A class of self-sustaining dissipative spherical dynamos. *Ann. Phys.* **4**, 372–447.

Braginsky, S. I. 1964 Kinematic models of the Earth's hydromagnetic dynamo. *Geomagnetism i Aeronomiya* **4**, 732. (English translation (1964) *Geomagnetism Aeronomy* **4**, 572–583.)

Bullard, E. C. & Gellman, H. 1954 Homogeneous dynamos and terrestrial magnetism. *Phil. Trans. R. Soc. Lond.* A **247**, 213–278.

Busse, F. H. 1970 Thermal instabilities in rotating systems. *J. Fluid Mech.* **44**, 444–460.

Dudley, M. L. & James, R. W. 1989 Time dependent dynamos with stationary flows. *Proc. R. Soc. Lond.* A **425**, 407–429.

Elsasser, W. M. 1946 Induction effects in terrestrial magnetism. Part I. Theory. *Phys. Rev.* **69**, 106–116.

Eltayeb, I. A. & Kumar, S. 1977 Hydromagnetic convective instability of a rotating self-gravitating fluid sphere containing a uniform distribution of heat sources. *Proc. R. Soc. Lond.* A **326**, 145–162.

Gilman, P. A. 1983 Dynamically consistent nonlinear dynamos driven by convection in a rotating spherical shell. II. Dynamos with cycles and strong feedbacks. *Astrophys. Geophys. Fluid Dyn.* **8**, 93–135.

Glatzmaier, G. A. & Roberts, P. H. 1995 A three-dimensional convective dynamo solution with rotating and finitely conducting inner core and mantle. *Phys. Earth Planet. Interiors* **91**, 63–75.

Golub, G. H. & Van Loan, C. F. 1989 *Matrix computations.* Baltimore, MD: Johns Hopkins University Press.

Gubbins, D. 1973 Numerical solutions of the kinematic dynamo problem. *Phil. Trans. R. Soc. Lond.* A **274**, 493–521.

Gubbins, D. & Roberts, P. H. 1987 Magnetohydrodynamics of the Earth's core. In *Geomagnetism* (ed. J. A. Jacobs), vol. II, ch. 1, pp. 1–183. Academic.

Gubbins, D. & Zhang, K. 1993 Symmetry properties of the dynamo equations for paleomagnetism and geomagnetism. *Phys. Earth Planet. Interiors* **75**, 225–241.

Herzenberg, A. 1958 Geomagnetic dynamos. *Phil. Trans. R. Soc. Lond.* A **250**, 543–583.

Hollerbach, R. 1996 On the theory of the geodynamo. *Phys. Earth Planet. Interiors* **98**, 163–185.

Hollerbach, R. & Jones, C. A. 1993 Influence of the Earth's inner core on geomagnetic fluctuations and reversals. *Nature* **365**, 541–543.

Holme, R. 1997 Three-dimensional kinematic dynamos with equatorial symmetry: application to the magnetic fields of Uranus and Neptune. *Phys. Earth Planet. Interiors* **102**, 105–122.

Hutcheson, K. A. & Gubbins, D. 1994 Kinematic magnetic field morphology at the core mantle boundary. *Geophys. J. Int.* **116**, 304–320.

Jacobs, J. A. 1987 *Geomagnetism*, vol. II. Academic.

Kuang, W. & Bloxham, J. 1997 An Earth-like numerical dynamo model. *Nature* **389**, 371–374.

Kumar, S. & Roberts, P. H. 1975 A three-dimensional kinematic dynamo. *Proc. R. Soc. Lond.* A **344**, 235–238.

Labrosse, S., Poirier, J.-P. & LeMouël, J.-L. 1997 On cooling of the Earth's core. *Phys. Earth Planet. Interiors* **99**, 1–17.

Lehoucq, R. B., Sorensen, D. C. & Yang, C. 1998 ARPACK *users guide: solution of large scale eigenvalue problems by implicitly restarted Arnoldi methods.* Philadelphia, PA: SIAM.

Lilley, F. E. M. 1970 On kinematic dynamos. *Proc. R. Soc. Lond.* A **316**, 153–167.

Love, J. & Gubbins, D. 1996 Dynamos driven by poloidal flows exist. *Geophys. Res. Lett.* **23**, 857–860.

Moffatt, H. K. 1970 Dynamo action associated with random inertial waves in a rotating conducting fluid. *J. Fluid Mech.* **44**, 705–719.

Moffatt, H. K. 1978 *Magnetic field generation in electrically conducting fluids.* Cambridge University Press.

Nakajima, T. & Kono, M. 1991 Kinematic dynamos associated with large scale fluid motions. *Geophys. Astrophys. Fluid Dyn.* **60**, 177–209.

Proctor, M. R. E. & Gilbert, A. D. 1994 *Stellar and planetary dynamos.* Cambridge University Press.

Proctor, M. R. E., Mathews, P. C. & Rucklidge, A. M. 1993 *Solar and planetary dynamos.* Cambridge University Press.

Roberts, G. O. 1972*a* Spatially periodic dynamos. *Phil. Trans. R. Soc. Lond.* A **266**, 535–558.

Roberts, P. H. 1972*b* Kinematic dynamo models. *Phil. Trans. R. Soc. Lond.* A **271**, 663–697.

Sarson, G. & Gubbins, D. 1996 Three-dimensional kinematic dynamos dominated by strong differential rotation. *J. Fluid Mech.* **306**, 223–265.

Sorensen, D. C. 1992 Implicit application of polynomial filters in a k-step Arnoldi method. *SIAM J. Matrix Analysis Appl.* **13**, 357–385.

Zhang, K.-K. & Busse, F. H. 1989 Convection driven magnetohydrodynamic dynamos in rotating spherical shells. *Geophys. Astrophys. Fluid Dyn.* **49**, 97–116.